SMART precision interferometry at 794 nm

John D. Monnier, Jean-Philippe Berger, Rafael Millan-Gabet, Wesley A. Traub, Nathaniel P. Carleton, et al.

John D. Monnier, Jean-Philippe Berger, Rafael Millan-Gabet, Wesley A. Traub, Nathaniel P. Carleton, Ettore Pedretti, Charles M. Coldwell, Costas D. Papaliolios, "SMART precision interferometry at 794 nm," Proc. SPIE 4838, Interferometry for Optical Astronomy II, (21 February 2003); doi: 10.1117/12.459696

SPIE.

Event: Astronomical Telescopes and Instrumentation, 2002, Waikoloa, Hawai'i, United States

SMART Precision Interferometry at 794 nm

J. D. Monnier[a,b], J.-P. Berger[a,c], R. Millan-Gabet[a,d], W. A. Traub[a], N. P. Carleton[a], E. Pedretti[a], C. M. Coldwell[e], and C. D. Papaliolios[e]

[a]Harvard-Smithsonian Center for Astrophysics, 60 Garden St, Cambridge, MA, 02138, USA
[b]University of Michigan, Astronomy Department
[c]Laboratoire d'Astrophysique de l'Observatoire de Grenoble
[d]Interferometry Science Center, California Institute of Technology
[e]Harvard University, Physics Department

ABSTRACT

Single-mode fibers have been used in the near-infrared to dramatically reduce calibration error for long-baseline interferometry. We have begun an effort to apply the advantages of spatial filtering at visible wavelengths for precision measurements of pulsating Cepheids using the IOTA interferometer. Rather than employing photometric taps to calibrate fluctuating coupling efficiency, we are using an "asymmetric" coupler which allows this calibration to be done without losing photons. The Single-Mode Asymmetric Recombination Technique (SMART) experiment has finished lab-testing, and has been installed at IOTA for full commissioning in Summer 2002. We report the results of lab characterization and first sky tests, as well as first fringes on a star using a visible-wavelength single-mode coupler. With both lab and sky experience using unpolarized light, we have found that circular silica fibers are quite practical for precision interferometric measurements. We conclude that circular fibers (as opposed to polarization maintaining fibers) have an undeserved poor reputation and that birefringence effects pose no significant difficulty.

Keywords: Fiber Optics, Optical Interferometry, Cepheids, Spatial Filtering

1. INTRODUCTION

This paper will discuss a practical implementation of an asymmetric coupler for optical interferometry, the SMART (Single-Mode Asymmetric Recombination Technique) experiment at the Infrared-Optical Telescope Array (IOTA). Monnier[1] introduced the idea of using an asymmetric coupler with single-mode fibers for exploiting the calibration advantages of spatial filtering[2–6] without losing light for the "photometric taps."

Following a brief theory section, we will document detailed characterization of the SMART experiment, including measurements of the commercial coupler and laboratory tests of the performance and stability. Next, we will describe practical experience at the IOTA interferometer, including the first reported astronomical fringes to be obtained using a single-mode coupler in the visible. Lastly, we will briefly describe our planned data analysis procedure and preliminary impressions of data quality.

2. THEORY

Here we only briefly introduce the theory behind the use of an asymmetric coupler; please consult Monnier[1] for detailed description as well as a signal-to-noise ratio comparison to the FLUOR combination scheme.[6]

Figure 1 shows the basic design of a asymmetric coupler for combining light for two telescopes. The coupler is defined so that the fraction α of F_1 is mixed with β of F_2 for interferometric output channel I_1, while the fraction β of F_1 is mixed with fraction α of F_2 for interference in I_2. If the coupler is loss-less, then $\beta = 1 - \alpha$,

Send correspondence to J.D.M. E-mail: monnier@umich.edu

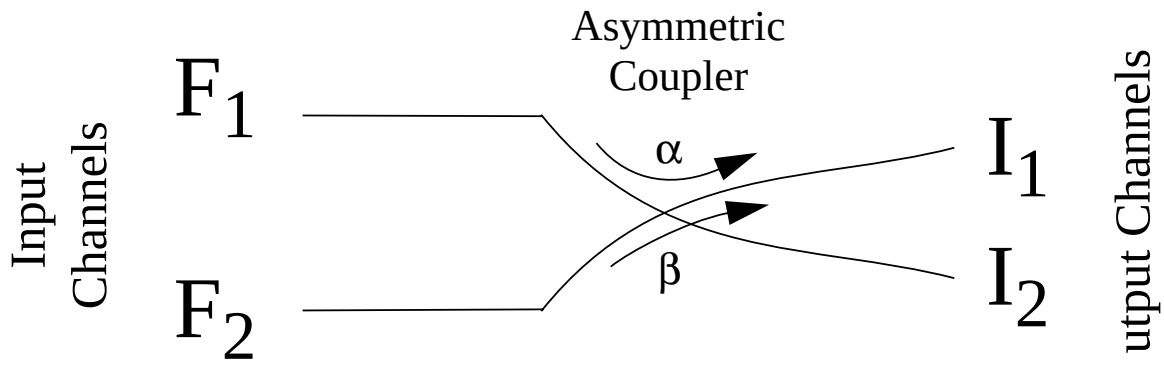

Figure 1.
This diagram illustrates the basic design of the asymmetric coupler being used in the SMART experiment. F_1 and F_2 represent the incoming fluxes from telescopes 1 and 2. These signals are coherently combined by the coupler and the optical fringes appear in the interferometric channels, I_1 and I_2. As shown in the figure, the fraction α (β) of F_1 (F_2) appears at I_1, while the fraction β (α) of F_1 (F_2) appears at I_2.

but we will keep the α and β notation for equation simplicity. To summarize, the outputs of the asymmetric coupler are given as:

$$I_1 = \alpha F_1 + \beta F_2 + 2\sqrt{\alpha F_1 \beta F_2} \cdot \gamma(t) \quad (1)$$

$$I_2 = \beta F_1 + \alpha F_2 - 2\sqrt{\alpha F_1 \beta F_2} \cdot \gamma(t) \quad (2)$$

In the last two equations, $\gamma(t)$ is the mutual coherence function and encodes the fringe visibility, the quantity we wish to measure. Usually γ is temporally modulated by adjusting the relative path lengths in the two arms of the interferometer. The amplitude of this modulation must be normalized by $2\sqrt{\alpha F_1 \beta F_2}$, thus arising the need to monitor the values of F_1 and F_2 for precise calibration.

In order to estimate the photometric flux from each telescope at the same time as we are detecting the fringe we must be able to estimate the incoherent part of the I-channels. This can be easily done by averaging these channels so that we remove the (modulated) fringe signal but not so long as to average out fluctuations due to the atmospheric fluctuations. This is generally straightforward since, as just mentioned, one needs to modulate the fringe at a frequency greater than the typical atmospheric time scale for accurate fringe amplitude measurements. We denote this incoherent component of the I-channels as $\langle I_i \rangle$, where the time-averaging is sufficient to remove the fringe component $\gamma(t)$ but not atmospheric fluctuations; this is equivalent to setting $\gamma(t) = 0$ in Eqs. (1) and (2).

Extracting F_i using an asymmetric coupler thus requires solving a system of two linear equations, involving $\langle I_1 \rangle$ and $\langle I_2 \rangle$. From inspection of Eqs. (1) and (2), we see that:

$$F_1 = \frac{\alpha \langle I_1 \rangle - \beta \langle I_2 \rangle}{\alpha^2 - \beta^2} \quad (3)$$

$$F_2 = \frac{\beta \langle I_1 \rangle - \alpha \langle I_2 \rangle}{\beta^2 - \alpha^2} \quad (4)$$

Note that these equations become indeterminate when $\alpha = \beta$, corresponding to the balanced coupler case, $\alpha = \frac{1}{2}$. This tells us that α must be significantly larger than β in order to avoid "amplifying" the measurement uncertainty when estimating F_i. See Figure 11 for an illustration of the procedure to extract photometric channel from linear combinations of the interferometric channels.

3. LABORATORY VALIDATION

3.1. Characteristics of Coupler

We acquired a single-mode coupler (fused biconical taper process) from Gould Fiber Optics (made with Corning Flexcor fiber equivalent, NA 0.14) which was advertised to be a 70%/30% asymmetric coupler (single-mode) at 780 nm, however the company did not provide any further information on the wavelength response. Using a near-infrared spectrometer, we measured the wavelength response of the coupler from approximately 700 nm to 1400 nm, and the results appear in Figure 2. The splitting ratio over a restricted range in wavelength relevant to this experiment is shown in Figure 3.

From this curve, we were able to determine the maximum usable bandpass for interferometry. If the coupling ratio changes too much inside the science bandpass, the measured fringe power becomes sensitive to the spectrum of the star being measured. Further, astrophysical interpretations can be hampered when using too broad a bandpass. We are using a high transmission (maximum 85%) bandpass filter by Spectro-Film which has a peak transmission at 794 nm and a FWHM 64 nm. This filter was used for both outputs of the coupler before detection, and the detailed bandpass shape can be found in Figure 4.

3.2. Description of Laboratory Interferometer

Figure 5 shows the optical layout of the lab interferometer. A bright white light source (Ocean Optics) is injected into a single-mode fiber, then re-launched as a 5 mm parallel beam. The beam encounters a 50/50 beamsplitter and dispersion compensation plate; the reflected light is directed towards a fiber focalization module where it is focused into one of the input fibers of the coupler. The transmitted beam reflects off a piezo-scanning mirror (Physik Instrumente) and then focused into the other input fiber of the coupler. One of the input fibers goes through a polarization controller (General Photonics) which can be used to match the birefringence of the two input fibers.

After combination in the coupler, light from each output fiber is re-collimated, filtered (Spectro-Film), then re-focused onto the 180 μm diameter active surface of an Avalanche Photo-Diode (APD, Perkin-Elmer Single-Photon Counting Module SPCM-AQR-13). Note that these latter optics do not need to be diffraction-limited, since the wavefronts have already been combined and the detector is large. The short "TTL-like" pulses from the SPCM are stretched out by a "One-Shot" circuit before being counted by a National Instruments counter

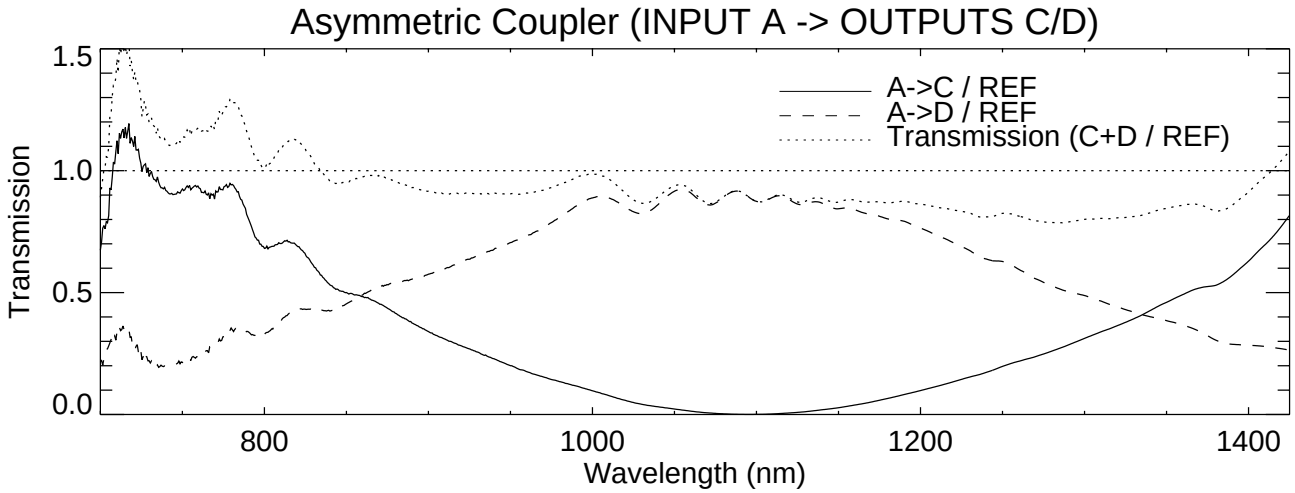

Figure 2. This figure shows the wavelength response of the asymmetric coupler used in the SMART experiment. A white-light source was injected into one of the input fibers (A) and the spectrum from each of the two coupler outputs C & D was measured. The solid line shows the transmission from input fiber A to output fiber C, normalized by the reference spectrum of the white light source. The dashed line shows the spectrum from output D.

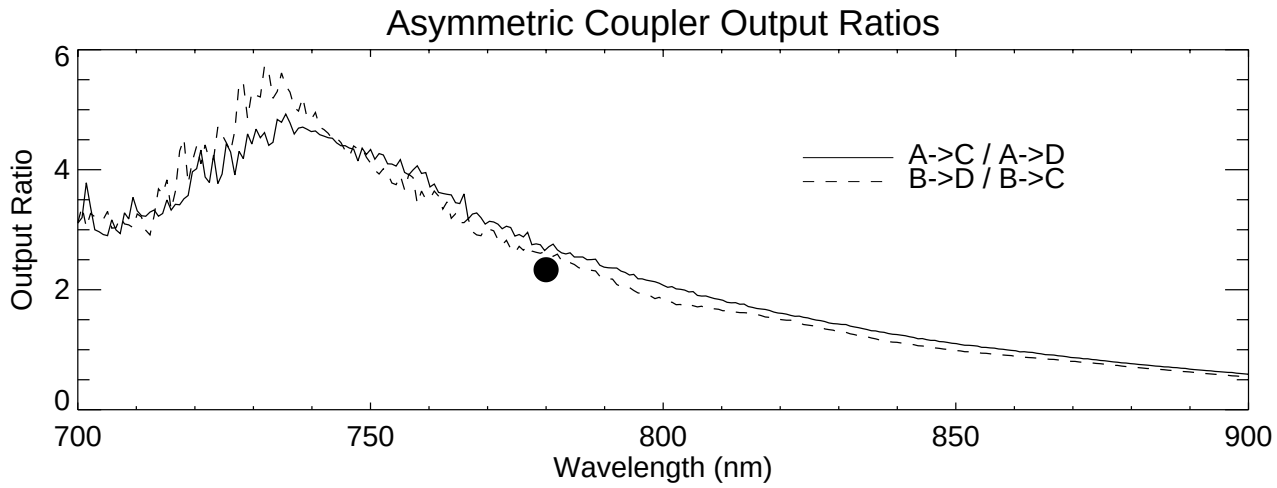

Figure 3. This figure shows the splitting ratio of the asymmetric coupler as a function of wavelength. The black dot shows the manufacturer specification at 780 nm, in reasonable agreement with our measurements. The two curves correspond to the two inputs fibers (A & B), and the difference between the curves is an estimate of the measurement uncertainty. The larger difference and fluctuations below 750 nm result from the fiber becoming multi-mode, thus more sensitive to handling during the measurement. This curve allows us to estimate the maximum bandwidth for the astronomical observations.

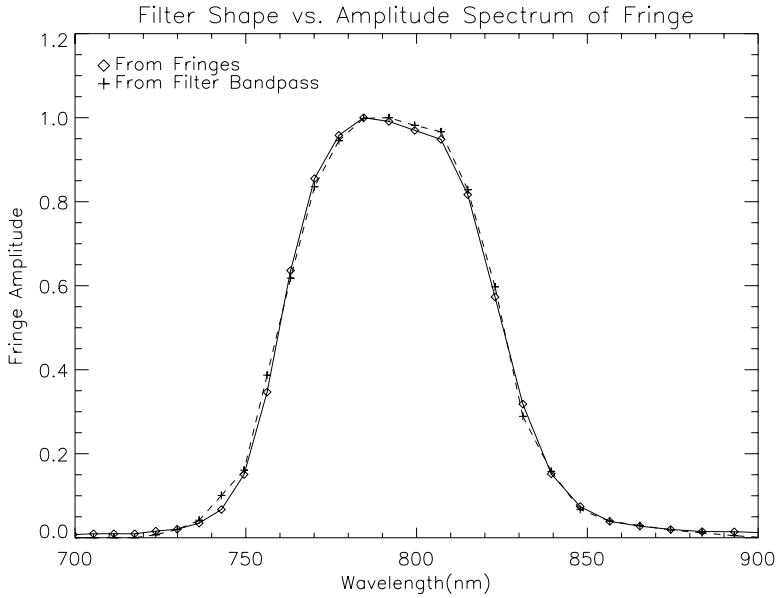

Figure 4.
This figure shows the bandpass of the science filter used by the SMART experiment. The two curves show both the spectrum from the manufacturer and the measured bandpass using Fourier Transform Spectroscopy in our lab.

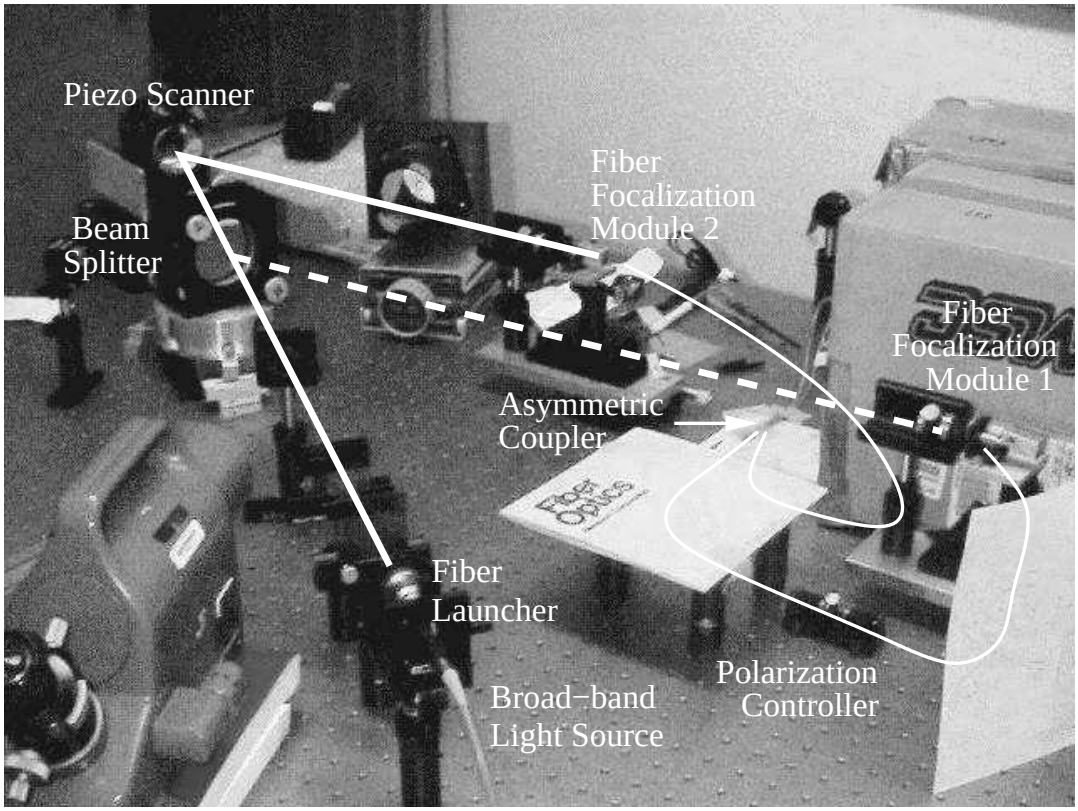

Figure 5. This diagram shows the setup of the laboratory interferometer. See text for detailed description.

board in a PC. Data recording and acquisition was done through C programs called from a basic graphical user interface.

3.3. Polarization Control

By equalizing the optical path difference (OPD) after the beamsplitter, the white light point was found and the broadband fringe was temporally modulated by scanning the OPD with the piezo scanner (60 μm stroke). We had expected the fringe visibility to be low before optimizing the polarization, but were surprised at the rather high initial contrast (>70%). We determined that this was because both input fibers followed similar curved paths in being connected to the focalization modules. By ensuring that similar turns and stresses were felt by both fibers, a reasonably high fringe contrast could be maintained in unpolarized light with no active polarization control. However, we were able to improve the contrast to above 90% by squeezing one of the input fibers using the General Photonics Pola-Rite polarization controller. See Figure 6 for an example laboratory fringe using a slightly broader bandpass filter (Andover) than the Spectro-Film filter which was ultimately used.

3.4. Dispersion

It is necessary to match the dispersion in the input fibers in order to have a high-contrast, broadband fringe. For a bandwidth of ~100 nm around 800 nm, we estimated that the fiber lengths had to be matched to better than 1 mm for typical silica fibers. This is not impossible but difficult when hand-connectorizing fibers, as we did in this experiment. We connectorized the coupler output fibers since the dispersion matching is not important after combination, but were reticent to attempt this for the input fibers. Instead we utilized temporary connectors (Bullet Bare Fiber adapters by Fiberplus International*). We laid out the input fibers and cleaved them to the

*Request metal, not plastic, components for connectors or the ferrule will not be rigidly held relative to the connector.

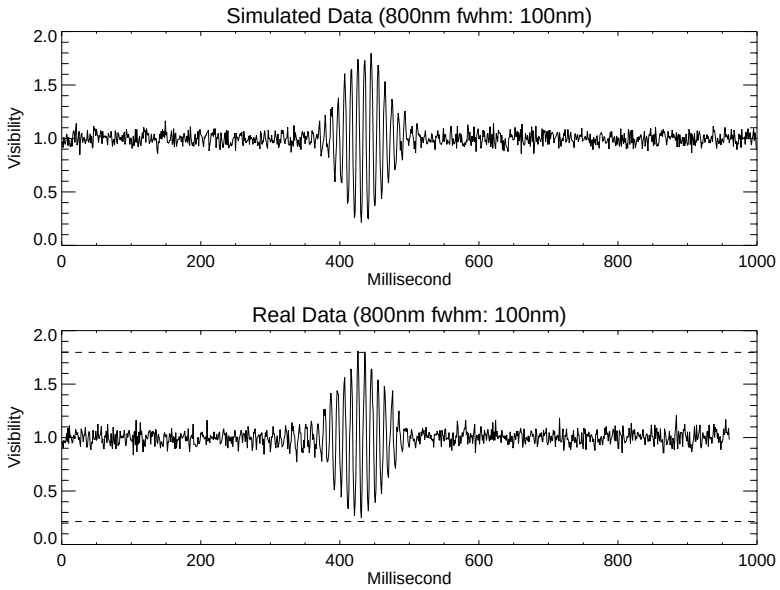

Figure 6.
Based on the measured coupler characteristics and filter properties (λ_0=800 nm, FWHM 100 nm) , we calculated and plotted *(top panel)* the theoretically expected fringe packet for our laboratory setup, including Poisson noise on the APD readout. This figure also shows *(bottom panel)* the measured laboratory fringe. The agreement is excellent, showing that the coupler does not suffer from significant mismatched dispersion or birefringence in the input fibers. Note the slight asymmetry of the laboratory fringe indicating a small amount of unmodeled dispersion inside this wide bandpass.

same length to within <1 mm. The cladding-stripped fiber end can be threaded through the Bullet Bare fiber adapter into a ceramic ferrule, and the fiber itself is secured by a spring-loaded clamp. The plan was to measure the dispersion matching of the fibers using the lab interferometer. If we needed to shorten one fiber, we would polish the fiber *in situ*, while being held by the Bullet Bare Fiber adapter (Fiberplus International claims this holder is secure enough).

However we found that we did not need to shorten the input fibers. Figure 7 shows the phase of the fringes as a function of wavelength. Unmatched dispersion would appear as a parabolic change of phase with wavelength. The small variation of phase with wavelength across the 62.5 nm bandpass indicates we cut the fibers to within 0.1 mm, a lucky accident.

3.5. Stability

Many workers warn of birefringence problems using circular waveguides made of silica.[3, 7–9] Small mechanical stresses indeed cause large changes in birefringence in the input fibers, which cause time-variable system visibilities, thus potentially negating the calibration advantages of spatial-filtering for unpolarized light. As discussed before, we were already surprised how benign the polarization mismatch problems were when care was taken to deploy the input fibers along parallel trajectories. As a further test, we measured laboratory fringes continuously for approximately two hours to see how much the contrast varied with time. Figure 8 shows the contrast exhibited negligible variations (<0.5%) during these tests.

Observing conditions at the IOTA inteferometer are much more hostile than the relatively stable temperature and atmosphere of a basement lab in Cambridge (although more modern combiner labs at NPOI, VLTI, CHARA are quite temperature stable). When making astronomical observations, we plan to interlace target star observations with calibrators in order to track system visibility changes on thermal timescales (~30 minutes). These tests shows the asymmetric coupler calibration can be remarkable stable, immune to mechanical relaxation of the fibers when not being manipulated, and insensitive to small temperature changes (a few degrees C).

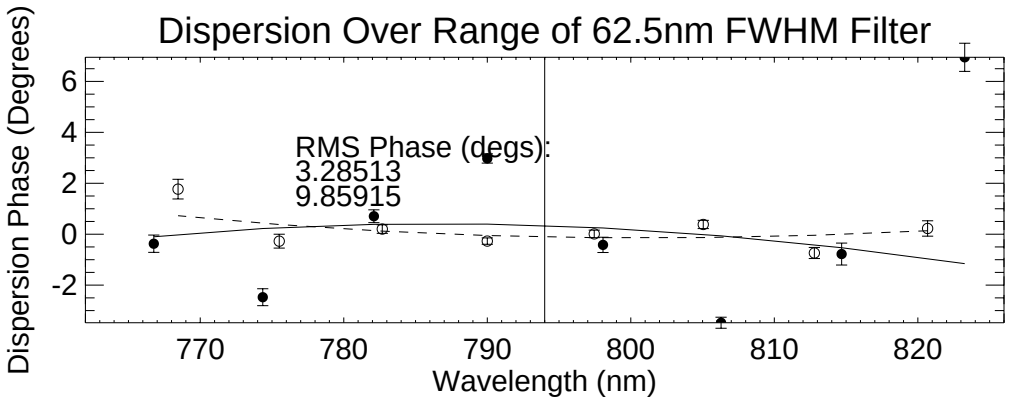

Figure 7.
This figure shows the fringe phase as function of wavelength, by using the laboratory scanning interferometer as a type of Fourier Transform Spectrometer. In the bandwidth of interest, the rms phase error is less than 4 deg (the two curves are for two different scanning directions), corresponding to a matched input fiber lengths of approximately 0.1 mm, assuming standard index of refraction for silica fibers. This will introduce negligible loss of visibility for astronomical observations between 765 nm and 820 nm.

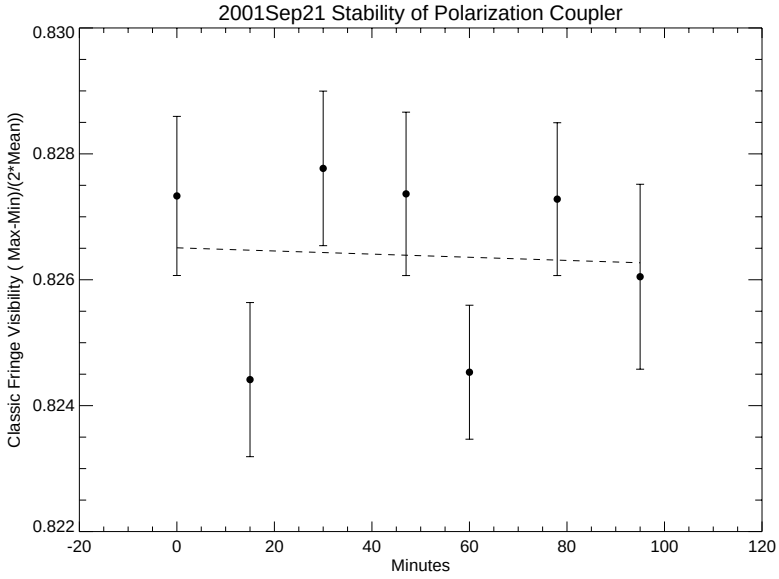

Figure 8.
This figure shows the stability of the fringe visibility over a period of nearly two hours under laboratory conditions. This shows that birefringence effects in silica (circular) fibers can be controlled at the level necessary for precision interferometry ($<< 1\%$). No polarizers were used for this or any of the results reported here.

4. PRACTICAL IMPLEMENTATION AT IOTA

4.1. Comments on Throughput and Sensitivity

Because the astronomical targets for the SMART experiment are relatively weak (V=4 mag), all aspects of this experiment were optimized to maximize the throughput for observations at the IOTA interferometer. Here is a list of crucial design elements which were necessary for attaining high sensitivity:

1. Custom dichroics (Janos Technologies) were used to reflect 99% of the light between 750 nm to 850 nm from the telescopes toward the focalization modules. The remainder of the visible light was transmitted and used by the startrackers for maximum tip-tilt correction of incoming wavefronts (servo loop at ∼200 Hz).
2. Shaklan[3] and Shaklan & Roddier[10] found that the maximum energy can be injected into a fiber when the aperture is approximately 4× r_0, where r_0 is the Fried parameter characterizing atmospheric turbulence. Typical r_0 in the visible is ∼10 cm, hence the full 45 cm apertures of the IOTA telescopes are approximately optimal in size for attaining maximum signal injection. After 10× beam compression at the telescope, the pupil is approximately 4.5 cm in diameter. For this experiment, we used 2 in clear aperture off-axis parabolas (OAP parent focal length 7.5 in, surface quality $\frac{\lambda}{5}$ peak-to-valley in Zerodur, manufactured by Nu-Tek) for focusing the full pupil into the single-mode fibers, with an f-ratio appropriate for the fiber's numerical aperture NA 0.14. While the OAPs are not diffraction-limited in the visible, it was determined that this has negligible effect on the fiber coupling because of the much larger wavefront perturbations induced by the atmosphere. This setup should maximize the injection into the fiber.
3. The polarization controller acts on the coupler input fiber itself (by squeezing and twisting), hence avoiding additional insertion loss if using a Babinet-Soleil style polarization compensator (or other external) module.
4. The coupler was specified to be low insertion loss (<0.4 dB) and low polarization cross-talk.
5. The light never has to travel longitudinally from one fiber to another, which would induce up to 0.6dB loss.
6. A high transmission filter was used (85%).
7. The optics used to collimate the output fiber light and focus onto the detector were both theoretically (with ZEMAX) and experimentally (with a lab CCD) verified to concentrate >95% of the energy onto the active area of the detector.
8. The SPCM-AQR-13 detector is arguably the most sensitive detector available for this application, with ∼60% photon detection efficiency at 800 nm and low dark count rate (<150 cts/s).

Figure 9 shows the light path from the telescopes toward the fast tip-tilt star trackers, and the optical path of the science light to the off-axis parabolas. Optical path length modulation is induced by a piezo-scanning platform (stroke 60μm) which holds the dichroic beamsplitters.

4.2. First Results on the Sky

On UT 2002 June 11 just after local midnight, we detected first fringes on α Oph. We immediately began taking data on our target star, the Cepheid η Aql which is significantly fainter. In Figure 10, we present fringes from a scan on the target η Aql attained on this first night of fringes. Both output channels are shown.

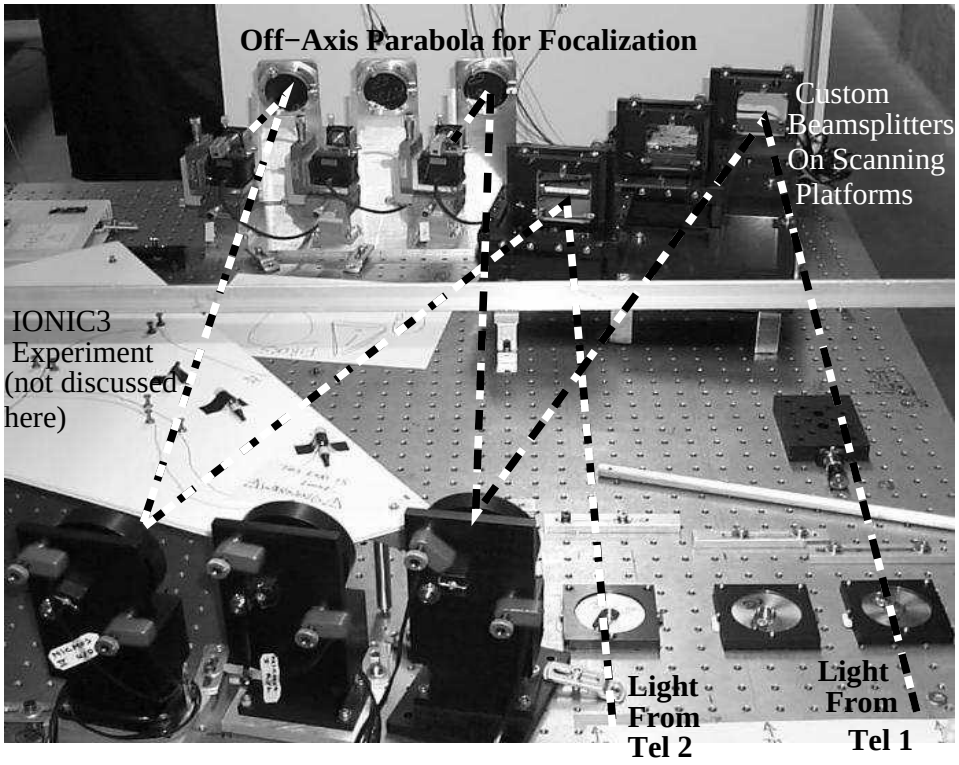

Figure 9. This figure shows the light path used at the IOTA interferometer to feed the asymmetric coupler. IOTA is a 3-telescope interferometer but only 2 of the beams are used for the SMART experiment. After traversing vacuum delay lines to compensate for sidereal motion, the beams exit the vacuum and enter the IOTA lab from the bottom of this figure. The science bandwidth reflects off the custom beamsplitters, while the rest of the visible photons continue to the fast tip-tilt system. The science beams are relayed by picomotor-adjustable mirrors before hitting the 2" diameter off-axis parabolas for focalization into the fibers.

4.3. Preliminary Data Analysis

Figure 11 illustrates the basic steps in a simple fringe analysis with an asymmetric coupler. After smoothing the interferometric channels, the photometric channels are reconstructed using previously measured coupler splitting ratios. In fact, we measure these splitting ratios for each source during each visit by taking data with alternating telescopes blocked. With the reconstructed photometric channels, we can remove the incoherent flux from the fringe scan and normalize the fringe amplitude, sample by sample.

After normalizing each fringe, the fringe "power" is measured by taking the power spectrum. This method is essentially the same method employed by the FLUOR experiment.[5, 6] The large fluctuations in the photometric signals in the visible cause bias problems when dividing by low amplitude fringe envelopes. In order to avoid this, we actually do not divide each fringe by the envelope, but rather calculate a single normalization factor for each scan which we use later to perform a weighted average of the power spectra. This method has the advantage of being insensitive to the above bias problem when the source and calibrator stars have different signal-to-noise ratios.

Unfortunately both of these methods are sensitive to piston fluctuations which occur during the scan,[11] and we are developing statistical methods to correct for this effect. Alternatively, one can fit the fringe in the time domain; this method has the advantage of allowing the piston fluctuations to be taken into account and does not require a bandpass correction factor for stars of different spectral types. However, time-domain fitting requires a much higher signal-to-noise ratio per scan than methods which average the power spectra.

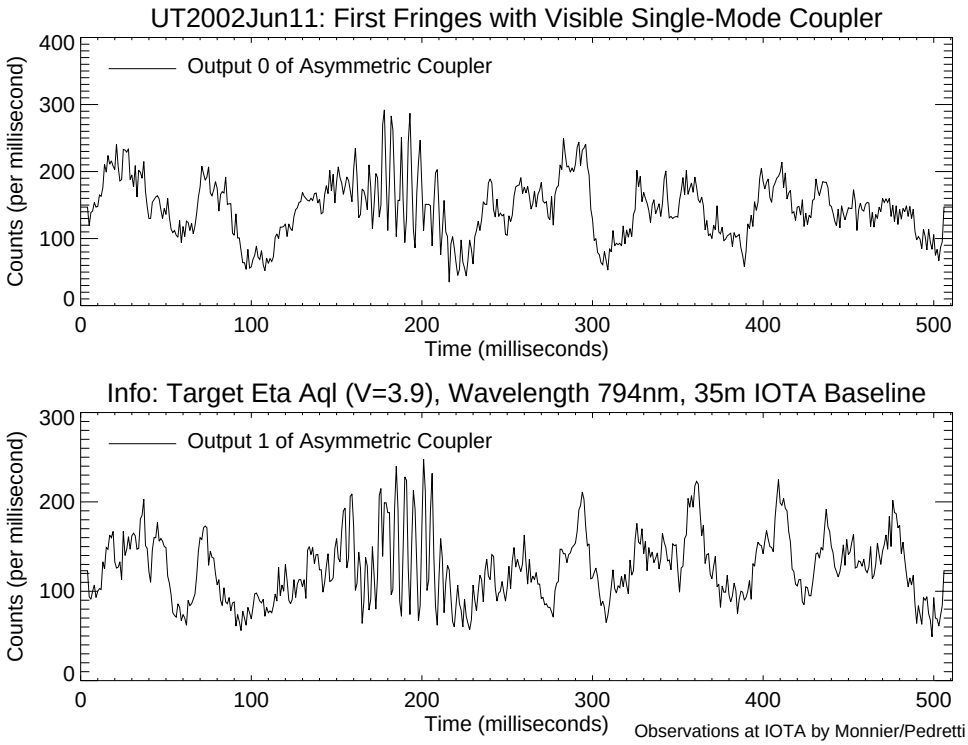

Figure 10.
This figure shows first sky fringes on the source η Aql on UT2002 Jun 11. The two panels correspond to the two outputs of the asymmetric coupler.

We have only just begun working with this new kind of data, and the final calibration precision achievable is not known. We have found that under average seeing we can estimate the fringe visibility of a V=4 mag star with a precision of less than 1% using only a few hundred scans (a few minutes of data). However, we do not yet know if these values are reproducible from night-to-night. Our first science paper will discuss in detail our data analysis method and calibrated visibility measurements from the full 2002 June run.

4.4. Good and Bad Seeing

Lastly, we want to comment on one interesting aspect of these observations. Because we are spatially filtering a pupil which is many times larger than the size of single coherent patch (r_0), the amount of light coupled into the fibers can fluctuate a large amount; this is strong function of the seeing. It is likely that data can be calibrated at the 1% level only during average or better seeing, since bad seeing varies so rapidly and dramatically. In Figure 12, we present two different fringes taken during both poor and good seeing. The difference is impressive.

5. CONCLUSIONS

We have reported on a novel experiment employing a single-mode asymmetric coupler for precision optical interferometry. We have carefully documented the wavelength and polarization performance, and found both to be significantly more benign than we had expected based on reports from other workers in the field.

We have demonstrated adequate throughput under real observing conditions at the IOTA interfometer, including first visible light fringes with single-mode fibers. We are currently pursuing precision measurements of changing diameters of pulsating stars. We expect that calibration of decoherence associated with piston fluctuations during fringe scans will be the dominant problem in the data analysis.

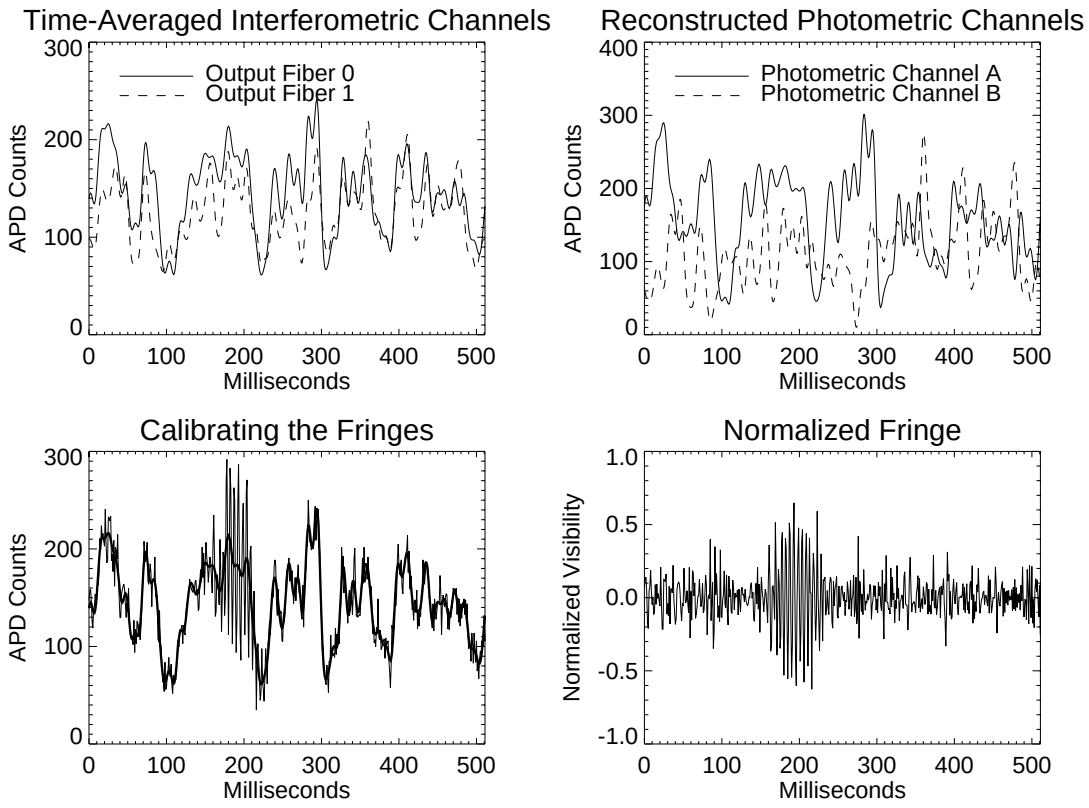

Figure 11. The top left panel shows the smoothed interferometric channels of the fringes shown in the previous figure. The top right panel shows the reconstructed photometric channels from each telescope based on the smoothed interferometric channels and the measured asymmetric coupling ratio. The bottom left panel shows the fringe from channel 0 and the mean photometric signal superimposed. The bottom right panel shows the final normalized fringes, having the mean flux removed and being normalized by the fringe envelope calculated from the instantaneous photometric channels.

ACKNOWLEDGMENTS

We thank J. Prohaska and the Center for Advanced Fiberoptic Applications for use of a spectrometer. JDM acknowledges the support of a Harvard-Smithsonian Center for Astrophysics Fellowship.

REFERENCES

1. J. D. Monnier, "Asymmetric Beam Combination for Optical Interferometry," PASP **113**, pp. 639–645, May 2001.
2. S. B. Shaklan and F. Roddier, "Single-mode fiber optics in a long-baseline interferometer," Appl. Opt. **26**, pp. 2159–2163, June 1987.
3. S. B. Shaklan, *Multiple Beam Correlation Using Single-Mode Fiber Optics with Application to Interferometric Imaging*. PhD thesis, The University of Arizona, 1989.
4. S. B. Shaklan, M. M. Colavita, and M. Shao, "Visibility Calibration Using Single-Mode Fibers in a Long-Baseline Interferometer," in *High-Resolution Imaging by Interferometry*, pp. 1287–+, 1992.
5. G. Perrin, V. Coude Du Foresto, S. T. Ridgway, J. Mariotti, and J. A. Benson, "Fibered recombination unit for the Infrared-Optical Telescope Array," in *Proc. SPIE Vol. 2476, p. 120-128, Fiber Optics in Astronomical Applications, Samuel C. Barden; Ed.*, **2476**, pp. 120–128, June 1995.
6. V. Coude Du Foresto, S. Ridgway, and J. . Mariotti, "Deriving object visibilities from interferograms obtained with a fiber stellar interferometer," A&AS **121**, pp. 379–392, Feb. 1997.

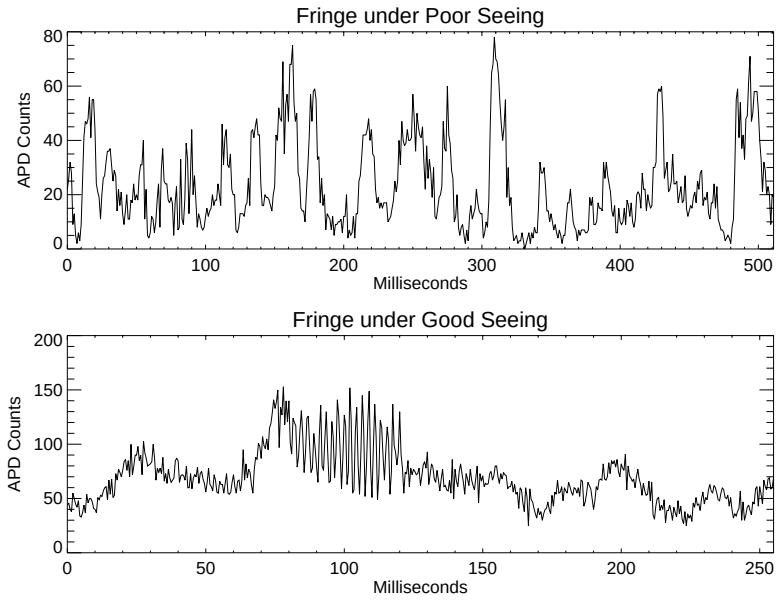

Figure 12. This figure shows fringe scans during poor and good seeing. Can you see the fringe near millisecond 90 in the first scan?

7. L. Delage and F. . Reynaud, "Analysis of polarisation requirements in a fiber-linked stellar interferometer," in *Integrated Optics for Astronomical Interferometry*, pp. 37+, 1997.
8. L. Delage and F. Reynaud, "Analysis and control of polarization effects on phase closure and image acquisition in a fibre-linked three-telescope stellar interferometer," *J. Opt. A: Pure Appl. Opt., Volume 2, Issue 2, pp. 147-153 (2000).* **2**, pp. 147–153, Mar. 2000.
9. R.-R. Rohloff and C. Leinert, "Properties of fiber optics for application in astronomical interferometry," Appl. Opt. **30**, pp. 5031–5036, Dec. 1991.
10. S. Shaklan and F. Roddier, "Coupling starlight into single-mode fiber optics," Appl. Opt. **27**, pp. 2334–2338, June 1988.
11. G. Perrin, "Correction of the "piston effect" in optical astronomical interferometry. I. Modulus and phase gradient of the visibility function restoration," A&AS **121**, pp. 553–568, Mar. 1997.